# Convex Nanobending at a Moving Contact Line: The Missing Mesoscopic Link in Dynamic Wetting

**Lei Chen,[†,‡,⊥] Jiapeng Yu,[†,⊥] and Hao Wang[*,†,§]**

[†]Laboratory of Heat and Mass Transport at Micro-Nano Scale, College of Engineering, Peking University, Beijing 100871, China, [‡]School of Mathematical Sciences, Peking University, Beijing 100871, China, and [§]Key Laboratory of Low-Grade Energy Utilization Technologies and Systems, Ministry of Education of China, Chongqing University, Chongqing 400044, China. [⊥]L. Chen and J. Yu contributed equally.

**ABSTRACT** The morphological information on the very front of a spreading liquid is fundamental to our understanding of dynamic wetting. Debate has lasted for years concerning the nanoscopic local angles and the transition from them to the macroscopic counterpart, $\theta_D$. This study of nonvolatile liquids analyzes the interface profile near the advancing contact line using an advanced atomic force microscopy. The interface is found following the macroscopic profile until bending in a convex profile around 20 nm from the substrate. This shoe-tip-like feature is common in partially wetting while absent for completely wetting, and its curvature varies with advancing speed. The observation ends the long-standing debate about the nanoscopic contact angles and their speed dependency. The convex nanobending provides a mesoscopic link and effectively complicates the dynamic wetting behaviors.

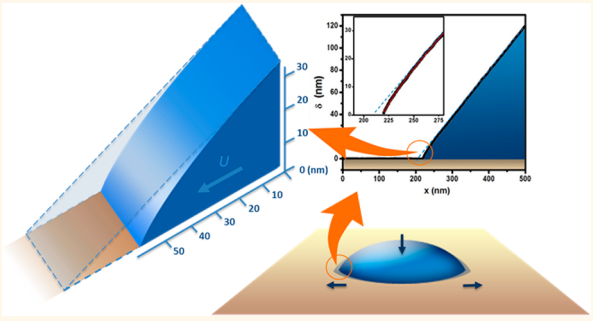


**KEYWORDS:** dynamic wetting · contact line · film profile · AFM · microscopic contact angle · mesoscopic contact angle · bending

Dynamic wetting is ubiquitous in natural and man-made systems. It plays important roles in large-scale systems, such as deposition,[1] coating,[2] and oil recovery,[3] and in small-scale systems such as electronics cooling,[4−6] micro- and nanofluidics,[7,8] self-assembly,[9,10] friction,[11] and various biological processes.[12−14] Being the junction of the triple-phase interfaces, the contact line is also a classic system for the study of long-range intermolecular forces, which are of central importance in nanotechnology.[15−18] Despite numerous efforts in recent decades, the precise wetting mechanisms remain vague, especially for partially wetting, which lacks precursor films.[19] Various hypotheses and theories have been proposed with the debate lasting for years regarding the contact line movement mechanism (molecule jumping, interface rolling, *etc.*), the regulation of the hydrodynamic singularity (slip, disjoining pressure, diffusion, *etc.*), and the correct model for predicting the profile and contact angles.[20−23]

An important reason for this situation is that the wetting process operates on a scale that extends from the macroscopic to the molecular, while our observations usually involve only macroscopic quantities measured at resolutions no better than several micrometers.[19] Model validation is then solely based on the fitting of the macroscopic contact angle, $\theta_D$, and the moving speed, $U$. Figure 1 depicts the various nanoscopic profiles proposed in different studies. The nanoscopic local angles could be smaller than, equal to, or greater than the macroscopic counterpart, $\theta_D$. Moreover, the microscopic contact angle, $\theta_m$, defined usually at a scale of nanometers from the contact line, is assumed either $U$ independent[19,24,25] or dependent[20,22,26] in different models, forming quite different bases for the mechanism as well as the model predictions.

Even for static liquids, the interface profile for film thicknesses less than 100 nm is difficult to measure since traditional optical methods are not applicable.[2,19,28] Electron microscopies that have been widely used for wettability studies at high spatial resolution include environmental scanning electron microscopy (ESEM),[29,30] wet scanning

* Address correspondence to hwang@coe.pku.edu.cn.

Received for review August 20, 2014 and accepted October 22, 2014.

**Published online October 22, 2014**
**10.1021/nn5046486**

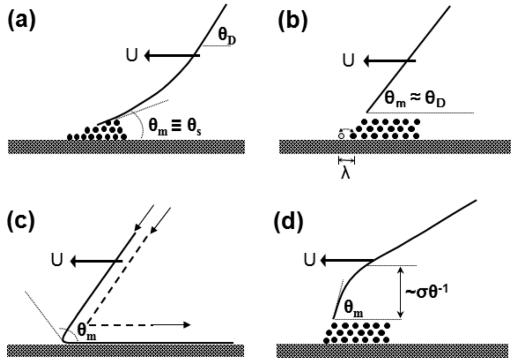


**Figure 1. Nanoscopic interface profiles proposed in different studies: (a) traditional hydrodynamic theory,[19,24,25] adapted from Bonn,[2] where $\theta_m$ is assumed to be a *U*-independent constant and the profile is concave; (b) molecular kinetic theory (MKT),[20] adapted from Blake,[19] where $\theta_m$ is assumed to be equal to $\theta_D$ and *U* dependent; (c) estimate based on interface rolling motion,[22,26] adapted from Shikhmurzaev;[22] (d) augmented hydrodynamic theory with van der Waals forces being taken into account, adapted from Gennes *et al.*,[27] where a convex bending emerges. $\sigma$ is about molecular size.**

transmission electron microscopy (wet-STEM),[31−33] and transmission electron microscopy (TEM).[34,35] Water condensation has been extensively studied through these methods.[29−33] The profile of a moving nanodroplet was also obtained,[32] but the driving force was an electron beam, which could deform the droplet into a toroidal shape.[33] On the other hand, tapping-mode atomic force microscopy (TM-AFM, also called intermittent contact mode AFM)[36] has been developed to be applicable to soft surfaces such as cells and liquids. The tip touches the sample gently at the end of each oscillation circle. The mechanical issues during the measurement have been answered by analyzing the interactions between the tip and the liquid surface.[37,38] Using TM-AFM on static liquids, a few pioneering studies have obtained the nanoscopic profiles near the contact line. For example, Herminghaus *et al.*[37,39] have resolved the film profiles of different liquids within 20 nm of a substrate. Ma *et al.*[40] measured contact angles of nanosized droplets. Yu *et al.*[41] measured the static contact angles about 100 nm from the substrate and proved that they are highly consistent with the optical results.

This work studies the partially wetting of nonvolatile liquids on flat solid substrates. The experimental system is based on a state-of-the-art TM-AFM (MFP-3D-BIO, Asylum Research), which has low-noise performance for high-resolution imaging of the most delicate samples such as proteins or liquid surfaces. It has shown excellent accuracy and stability in a previous study on static droplets[41] compared with optical methods. Improvements have been made by moving the test section into a chamber, where the atmosphere (pure nitrogen), temperature (25 °C), and electrostatic level are well controlled, and by employing a probe with a sharp tip with a radius of less than

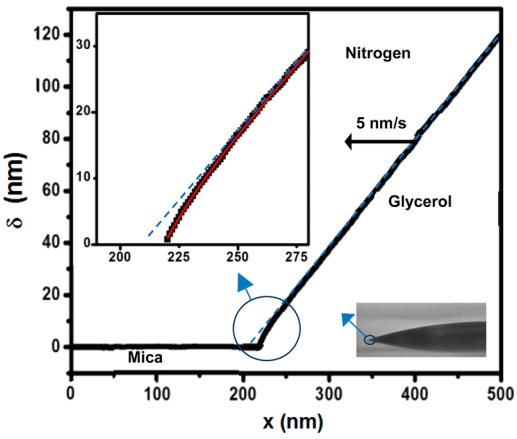


**Figure 2. Measured nanoscopic profile near the advancing contact line of a glycerol droplet on mica. The advancing speed is 5 nm/s leftward. The inset shows the details near the contact line. The dashed lines are straight to illustrate the bending.**

10 nm (AC-240, Olympus). The unsolved region at the very corner of the contact line due to the finite tip size is at maximum 3.6, mostly 2 nm, from the substrate. The scan size is 1000 nm in *x*, and therein are 512 data points. See Supporting Information for a detailed description of the imaging method and the error analysis.

## RESULTS AND DISCUSSION

We obtain the interface profile within 100 nm of the substrate as shown in Figure 2. The interface is the very front of a millimeter-sized glycerol droplet in its final stage of spreading. *U* is 5 nm/s leftward, and the spreading lasts for minutes around this rate. The profile is seen to extend as a straight line from the bulk liquid downward, which follows the macroscopic profile, until it bends backward in a convex shape about 20 nm from the substrate. The detailed shape is shown in the inset. The convex bending is more obvious as the profile approaches the substrate. The tendency does not change even down to a thickness of 2 nm, which is about the limit of the measurement.

The convex bending within 20 nm of the substrate is found to be common in nonvolatile partially wetting systems. The tested liquids include glycerol, polyethylene glycol (with a molecular weight of 400, PEG 400), silicone oil (viscosity 0.001 $m^2/s$), and phosphoric acid (85% weight). The solid substrates include mica, contaminated mica (by exposure in air for 24 h), polystyrene (PS), polydimethylsiloxane (PDMS), and silicon. Convex bending has been seen in all of the partially wetting cases (glycerol on PS and PDMS is not measured because the contact angle is so big that the droplet height exceeds the probe capability). Three examples are shown in Figure 3a−c. The bending profiles are all within about 20 nm of the substrate and are even more obvious within about 10 nm. Similar results are obtained for inorganic fluids such as phosphoric acid (85% weight) on silicon.

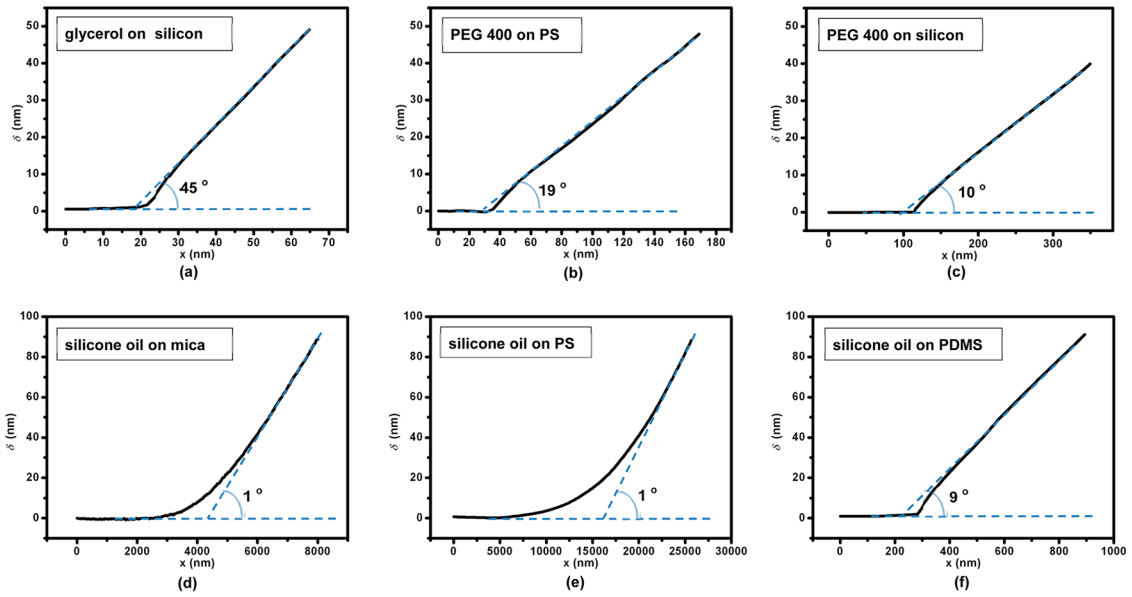


**Figure 3. Nanoscopic profiles near the advancing contact line of nonvolatile liquids (*U* ranges from 5 to 10 nm/s): (a–c) partially wetting of glycerol or PEG 400 on silicon or PS; (d, e) completely wetting of silicon oil on mica and PS without convex bending being observed; (f) partially wetting of silicon oil on PDMS with convex bending.**

In contrast, convex bending is not seen in any completely wetting cases. Figure 3d,e show silicon oil completely wetting on mica or PS. There is no convex bending but a rather flat profile with a slightly concave shape, which is consistent with theories for completely wetting.[2] Convex bending occurs, however, when the substrate is switched to PDMS, which has a very low surface energy, making the silicon oil partially wet, as seen in Figure 3f.

The speed dependency of the nanoscopic profiles has also been investigated. The convex bending is dependent on the contact line motion. Figure 4a compares the profiles at $U$ = 30 and 3 nm/s for glycerol on mica. The local $\theta$ as well as the bending curvature increases with $U$. Figure 4b summarizes the variation of local $\theta$ for three different thicknesses (4, 10, and 100 nm) in a same test case. It is seen that the three angles all increase as $U$ increases, but that for the 4 nm thickness has the greatest increasing rate and that for the 100 nm thickness has the lowest increasing rate, which means closer to the contact line $\theta$ is more dependent on $U$. For the equilibrium droplets with static contact lines (it usually takes more than 1 day for the glycerol droplets to reach an equilibrium state), the film profiles are nearly straight down to the substrate. The local contact angles along the profile are about the same value, as shown in Figure 4b.

The observation answers long-standing puzzles about the nanoscopic angles and their $U$ dependency. A well-known traditional hydrodynamic theory, the Cox–Voinov law, focuses on the viscous losses in the liquid wedge.[19,24,25] The local angle along the profile is determined by

$$\theta^3 - \theta_m^3 = 9\mathrm{Ca}\ln\left(\frac{L}{L_m}\right), \quad \mathrm{Ca} = U\frac{\eta}{\gamma} \qquad (1)$$

where $L_m$ according to the theory is the scale of the microscopic region and $\theta_m$ is extracted at $L_m$. An important assumption is that $\theta_m$ is $U$ independent, equal to the static angle, $\theta_s$. As a consequence, $\theta$ has to be less and less dependent on $U$ when closer to the contact line, exactly opposite the present observation. In the literature the assumption has been debated for years.[24]

The profile determined by eq 1 is concave, as depicted in Figure 1a,[2,19] as the right side of eq 1 is always positive. The linear profile beyond the convex bending, on the other hand, is consistent with the theory, because in our experiments $U$ is so small that the right side of eq 1 is about zero; thus $\theta = \theta_m$.

Another broadly used theory, the MKT, is based on the molecular displacement at the moving contact line as depicted in Figure 1b, in which $\theta$ is naturally coupled to $U$:[20]

$$U = 2\kappa^0\lambda\sinh[\gamma(\cos\theta_s - \cos\theta)\lambda^2/2k_BT] \qquad (2)$$

which fits well with nanoscopic $\theta$ data for different thicknesses as shown in Figure 4b, yet with different fitting parameters, *i.e.*, the microscopic molecular displacement distance, $\lambda$, and the jump frequency, $\kappa^0$. In Shikhmurzaev's model, which is based on the concept of interface rolling, local $\theta$ is also naturally coupled to $U$.[22,26] The fitting performance of the simplified expression by Shikhmurzaev[22,42] is as good as that of the MKT.

The MKT simply assumes no bending, as depicted in Figure 1b. Gennes *et al*. has proposed that the disjoining pressure induced by van der Waals forces could bend the profile near the contact line.[27] Their prediction as depicted in Figure 1d is quite similar to the

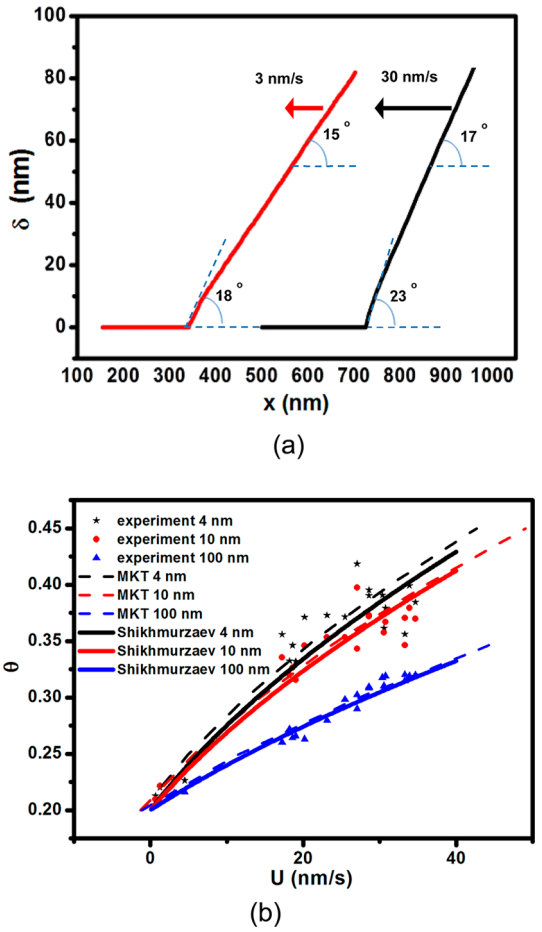


**Figure 4. *U* dependency of the nanoscopic profiles: (a) Comparison of profiles at two speeds for glycerol on mica. The faster one has greater local angles and bending curvature. (b) Comparison of *U* dependencies of the local contact angles for different thicknesses (4, 10, and 100 nm), with the fittings of the MKT[20] and Shikhmurzaev's model.[22,42] The local angle closest to the contact line has the greatest increasing rate with *U*.**

present observation. However, the bending thickness scale, $\sigma\theta^{-1}$ as depicted in Figure 1d,[39] is hardly beyond 2 nm, which is already about the limit of our measurement. Even more problematic, this theory suggests a constant bending that exists even at a static state, which is not consistent with the observed dynamic characteristics of the bending.

The convex bending provides an ever-missing link between the molecular and the macroscopic in dynamic wetting theories. The liquid structure near an advancing contact line could be sketched as in Figure 5 with four regions involved. Closest to the contact

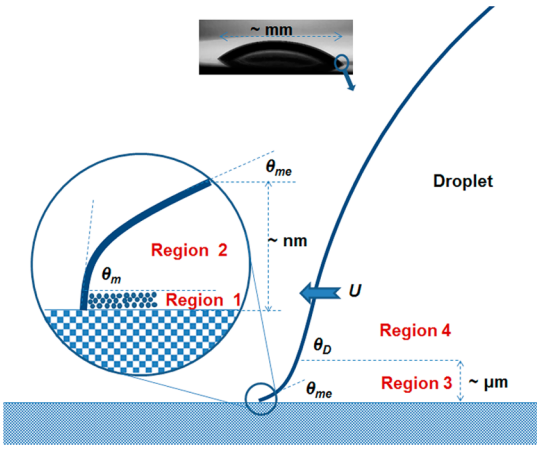


**Figure 5. Schematic diagram of the liquid structure at the advancing contact line of partially wetting liquids. Regions 1 to 4 are the molecular region, convex bending (which is convex), viscous bending, and macroscopic region, respectively. The microscopic contact angle, $\theta_m$, varies with the moving speed according to the MKT. The mesoscopic contact angle, $\theta_{me}$, is established at the end of the convex bending.**

line is the molecular region of layers of molecules. The microscopic contact angle, $\theta_m$, is established at the end of this region according to the MKT. Then it is the observed convex bending region, followed by a viscous bending region.

Three important local angles are featured at the junctions of the four regions, *i.e.*, $\theta_m$, $\theta_D$, and $\theta_{me}$, which is at the end of the convex bending. We name $\theta_{me}$ the mesoscopic contact angle since it is located between the microscopic and the macroscopic one. Away from the contact line, the local angle drops from $\theta_m$ to $\theta_{me}$ and then increases to $\theta_D$. The convex bending is unique since it provides a mechanism that allows the angle to drop along the profile.

## CONCLUSIONS

This article describes the nanoscopic interface profile near the contact line for nonvolatile liquids during partially wetting. The key feature is a shoe-tip-like bending region within 20 nm of the substrate. The bending profile varies systematically with the advancing speed. The observation ends the long-standing debate about the speed dependency of the nanoscopic contact angles. The bending provides the missing link from the molecular to the macroscopic. A four-region partition scheme is proposed to describe the liquid structure at the advancing contact line of partially wetting liquids.

## METHODS AND EXPERIMENTAL SECTION

The experimental system is based on a state-of-the-art TM-AFM (MFP-3D-BIO, Asylum Research). The probe has a sharp tip of radius less than 10 nm (AC-240, Olympus). The resonance frequency of the probe is about 70 kHz, and the spring constant is about 2 N/m. The scan speed of the tip is 200 nm/s.

Amplitude modulation is employed during the measurement. The imaging technique consists in driving the cantilever just off its fundamental resonant frequency at some user-defined amplitude set point. The feedback loop maintains this set point amplitude (voltage) as the tip scans across the surface, retracting the Z piezo when the amplitude gets dampened (over bumps) or

extending the Z piezo when/if it oscillates at a larger amplitude than the amplitude set point (over holes). The free air amplitude of the tip is 700 mV. The set point and the integer gain are chosen such that the tip works at the attractive region (phase lag >90°) and thus has a gentle interaction with the sample surface.[43] The energy dissipated by the tip−sample interaction is calculated to be less than 0.05 pW, thus is negligible.[43] Analysis based on the force−distance curve shows that the displacement of the local liquid profile due to tip disturbance is less than 1 nm. The highly linear and smooth liquid profiles obtained in the tests also indicate that the sample is not distorted by the tip. On the other hand, the experimental errors mainly come from tip−sample convolution effects due to the finite size of the tip. The convolution results in an overall dilation of the profile and an unresolved region near the contact line. The deconvolution analysis[44] shows that the dilation is negligible since the caused error on the local angle measurement is no more than 0.5°. The unsolved region at the very corner of the contact line due to the finite tip size is at most 3.6 nm from the substrate. See Supporting Information for a detailed description of the imaging method and the error analysis. During the measurement the probe alignment is adjusted to ensure that the scanning direction, *x*, is perpendicular to the contact line. The probe scans forward to obtain the trace data and then immediately reverses to obtain the retrace data. The trace and retrace data are processed to obtain the real profile. See Supporting Information for a detailed derivation.

*Conflict of Interest:* The authors declare no competing financial interest.

*Acknowledgment.* This work was supported by the National Natural Science Foundation of China (No. 91334110, 50706001) and Key Laboratory of Low-Grade Energy Utilization Technologies and Systems, Ministry of Education of China (No. LLEUTS 201302). The authors acknowledge stimulating discussions with Dr. Terence D. Blake at the University of Mons-Hainaut and Dr. Xiaodong Wang at North China Electric Power University.

*Supporting Information Available:* (1) Error analysis and deconvolution and (2) measurement on advancing films. This material is available free of charge *via* the Internet at http://pubs.acs.org.

## REFERENCES AND NOTES

1. Bergeron, V.; Bonn, D.; Martin, J. Y.; Vovelle, L. Controlling Droplet Deposition with Polymer Additives. *Nature* **2000**, *405*, 772–775.
2. Bonn, D.; Eggers, J.; Indekeu, J.; Meunier, J.; Rolley, E. Wetting and Spreading. *Rev. Mod. Phys.* **2009**, *81*, 739–805.
3. Bertrand, E.; Bonn, D.; Broseta, D.; Dobbs, H.; Indekeu, J.; Meunier, J.; Ragil, K.; Shahidzadeh, N. Wetting of Alkanes on Water. *J. Petrol. Sci. Eng.* **2002**, *33*, 217–222.
4. Wang, H.; Garimella, S. V.; Murthy, J. Y. Characteristics of an Evaporating Thin Film in a Microchannel. *Int. J. Heat Mass Transfer* **2007**, *50*, 3933–3942.
5. Miljkovic, N.; Preston, D. J.; Enright, R.; Wang, E. N. Electrostatic Charging of Jumping Droplets. *Nat. Commun.* **2013**, 4.
6. Boreyko, J. B.; Chen, C. H. Self-Propelled Dropwise Condensate on Superhydrophobic Surfaces. *Phys. Rev. Lett.* **2009**, *103*, 184501.
7. Yunker, P. J.; Still, T.; Lohr, M. A.; Yodh, A. G. Suppression of the Coffee-Ring Effect by Shape-Dependent Capillary Interactions. *Nature* **2011**, *476*, 308–311.
8. Seemann, R.; Brinkmann, M.; Kramer, E. J.; Lange, F. F.; Lipowsky, R. Wetting Morphologies at Microstructured Surfaces. *Proc. Natl. Acad. Sci. U.S.A.* **2005**, *102*, 1848–1852.
9. Grouchko, M.; Roitman, P.; Zhu, X.; Popov, I.; Kamyshny, A.; Su, H.; Magdassi, S. Merging of Metal Nanoparticles Driven by Selective Wettability of Silver Nanostructures. *Nat. Commun.* **2014**, *5*.
10. Deegan, R. D.; Bakajin, O.; Dupont, T. F.; Huber, G.; Nagel, S. R.; Witten, T. A. Capillary Flow as the Cause of Ring Stains from Dried Liquid Drops. *Nature* **1997**, *389*, 827–828.
11. Klein, J.; Perahia, D.; Warburg, S. Forces between Polymer-Bearing Surfaces Undergoing Shear. *Nature* **1991**, *352*, 143–145.
12. Leiske, D. L.; Monteux, C.; Senchyna, M.; Ketelson, H. A.; Fuller, G. G. Influence of Surface Rheology on Dynamic Wetting of Droplets Coated with Insoluble Surfactants. *Soft Matter* **2011**, *7*, 7747–7753.
13. Sansom, M. S.; Biggin, P. C. Biophysics: Water at the Nanoscale. *Nature* **2001**, *414*, 156–159.
14. Roth-Nebelsick, A.; Ebner, M.; Miranda, T.; Gottschalk, V.; Voigt, D.; Gorb, S.; Stegmaier, T.; Sarsour, J.; Linke, M.; Konrad, W. Leaf Surface Structures Enable the Endemic Namib Desert Grass Stipagrostis Sabulicola to Irrigate Itself with Fog Water. *J. R. Soc. Interface* **2012**, *9*, 1965–1974.
15. Shih, C.-J.; Strano, M. S.; Blankschtein, D. Wetting Translucency of Graphene. *Nat. Mater.* **2013**, *12*, 866–869.
16. Zeng, Y.; von Klitzing, R. Structuring of Colloidal Suspensions Confined between a Silica Microsphere and an Air Bubble. *Soft Matter* **2011**, *7*, 5329–5338.
17. Barrat, J. L. A Possible Mechanism for Swelling of Polymer Brushes under Shear. *Macromolecules* **1992**, *25*, 832–834.
18. Israelachvili, J. N. *Intermolecular and Surface Forces*, 3rd ed.; Academic Press, 2011.
19. Blake, T. D. The Physics of Moving Wetting Lines. *J. Colloid Interface Sci.* **2006**, *299*, 1–13.
20. Blake, T.; Haynes, J. Kinetics of Liquid Liquid Displacement. *J. Colloid Interface Sci.* **1969**, *30*, 421–423.
21. Wayner, P. C., Jr. Spreading of a Liquid Film with a Finite Contact Angle by the Evaporation/Condensation Process. *Langmuir* **1993**, *9*, 294–299.
22. Shikhmurzaev, Y. D. Moving Contact Lines in Liquid/Liquid/Solid Systems. *J. Fluid Mech.* **1997**, *334*, 211–249.
23. Qian, T.; Wang, X.-P.; Sheng, P. A Variational Approach to Moving Contact Line Hydrodynamics. *J. Fluid Mech.* **2006**, *564*, 333–360.
24. Voinov, O. Hydrodynamics of Wetting. *Fluid Dyn.* **1976**, *11*, 714–721.
25. Cox, R. The Dynamics of the Spreading of Liquids on a Solid Surface. Part 1. Viscous Flow. *J. Fluid Mech.* **1986**, *168*, 169–194.
26. Shikhmurzaev, Y. D. The Moving Contact Line on a Smooth Solid Surface. *Int. J. Multiphase Flow* **1993**, *19*, 589–610.
27. Gennes, P. G. D.; Hua, X.; Levinson, P. Dynamics of Wetting: Local Contact Angles. *J. Fluid Mech.* **1990**, *212*, 55–63.
28. Zheng, L.; Wang, Y. X.; Plawsky, J. L.; Wayner, P. C. Accuracy of Measurements of Curvature and Apparent Contact Angle in a Constrained Vapor Bubble Heat Exchanger. *Int. J. Heat Mass Transfer* **2002**, *45*, 2021–2030.
29. Miljkovic, N.; Enright, R.; Nam, Y.; Lopez, K.; Dou, N.; Sack, J.; Wang, E. N. Jumping-Droplet-Enhanced Condensation on Scalable Superhydrophobic Nanostructured Surfaces. *Nano Lett.* **2012**, *13*, 179–187.
30. Rykaczewski, K. Microdroplet Growth Mechanism during Water Condensation on Superhydrophobic Surfaces. *Langmuir* **2012**, *28*, 7720–7729.
31. Barkay, Z. Wettability Study Using Transmitted Electrons in Environmental Scanning Electron Microscope. *Appl. Phys. Lett.* **2010**, 96.
32. Barkay, Z. Dynamic Study of Nanodroplet Nucleation and Growth on Self-Supported Nanothick Liquid Films. *Langmuir* **2010**, *26*, 18581–18584.
33. Rykaczewski, K.; Scott, J. H. J. Methodology for Imaging Nano-to-Microscale Water Condensation Dynamics on Complex Nanostructures. *Nano* **2011**, *5*, 5962–5968.
34. Mirsaidov, U. M.; Zheng, H.; Bhattacharya, D.; Casana, Y.; Matsudaira, P. Direct Observation of Stick-Slip Movements of Water Nanodroplets Induced by an Electron Beam. *Proc. Natl. Acad. Sci. U.S.A.* **2012**, *109*, 7187–7190.
35. Leong, F. Y.; Mirsaidov, U. M.; Matsudaira, P.; Mahadevan, L. Dynamics of a Nanodroplet under a Transmission Electron Microscope. *Phys. Fluids* **2014**, 26.
36. García, R.; Perez, R. Dynamic Atomic Force Microscopy Methods. *Surf. Sci. Rep.* **2002**, *47*, 197–301.
37. Herminghaus, S.; Pompe, T.; Fery, A. Scanning Force Microscopy Investigation of Liquid Structures and Its Application to Fundamental Wetting Research. *J. Adhes. Sci. Technol.* **2000**, *14*, 1767–1782.

38. Mugele, F.; Becker, T.; Nikopoulos, R.; Kohonen, M.; Herminghaus, S. Capillarity at the Nanoscale: An Afm View. *J. Adhes. Sci. Technol.* **2002**, *16*, 951–964.
39. Pompe, T.; Herminghaus, S. Three-Phase Contact Line Energetics from Nanoscale Liquid Surface Topographies. *Phys. Rev. Lett.* **2000**, *85*, 1930.
40. Ma, J.; Jing, G.; Chen, S.; Yu, D. Contact Angle of Glycerol Nanodroplets under Van Der Waals Force. *J. Phys. Chem. C* **2009**, *113*, 16169–16173.
41. Yu, J.; Wang, H.; Liu, X. Direct Measurement of Macro Contact Angles through Atomic Force Microscopy. *Int. J. Heat Mass Transfer* **2013**, *57*, 299–303.
42. Blake, T. D.; Shikhmurzaev, Y. D. Dynamic Wetting by Liquids of Different Viscosity. *J. Colloid Interface Sci.* **2002**, *253*, 196–202.
43. Cleveland, J.; Anczykowski, B.; Schmid, A.; Elings, V. Energy Dissipation in Tapping-Mode Atomic Force Microscopy. *Appl. Phys. Lett.* **1998**, *72*, 2613–2615.
44. Keller, D. J.; Franke, F. S. Envelope Reconstruction of Probe Microscope Images. *Surf. Sci.* **1993**, *294*, 409–419.